Handling Method for Outages of IGS Real-Time Service (RTS) in GNSS Real-Time Sensing of Atmospheric Water Vapor

HaoJun Li, XiaoMing Li, and Qi Kang, *Senior Member, IEEE*

***Abstract*—The continuity and accuracy of real-time (RT) global satellite navigation system (GNSS) sensing of atmospheric water vapor can be seriously affected by a lack of connectivity. To mitigate this issue, a method has been developed that utilizes the International GNSS Service (IGS) ultrarapid satellite orbit and an established RT service (RTS) for satellite clock correction. This method ensures the accuracy of RT atmospheric water vapor estimation even when communication is interrupted. The established RTS utilizes variations in historical clock correction data from the user side to extrapolate its RT high-precision value. Through experimentation, it has been determined that using a quadratic polynomial and an eighth-order harmonic-based function along with 1-h historical clock correction data is optimal for establishing this RTS method. The 2-D and 3-D accuracies of static Precise Point Positioning can achieve centimeter to millimeter levels, and the estimated average root mean square (rms) of zenith tropospheric delay (ZTD) is equivalent to the RT archived products. When compared to the precipitable water vapor results obtained from IGS ZTD products, the averaged rms values of GPS, Galileo, and BDS-3 PWV reach 3.12, 4.41, and 6.43 mm, respectively, which can meet the accuracy requirements of general numerical weather forecasting and other applications during communication interruptions.**

***Index Terms*—Precipitable water vapor (PWV), precise point positioning (PPP), real-time service (RTS), satellite clock error corrections.**

I. Introduction

THE global satellite navigation system (GNSS) precise point positioning (PPP) has been widely used for various applications [1], [2], [3] including atmospheric water vapor sensing [4], [5], [6], earthquake, and deformation monitoring [7], [8], [9]. The GNSS sensing of atmospheric water vapor is highly related to precipitable water vapor (PWV), which is usually computed by zenith wet delay (ZWD) derived from PPP processing [4], [10] and weighted mean temperature [11], [12]. PPP computation utilizes single-receiver dual-frequency phase and range observations, as well as high-precision satellite clock and orbit products provided by the International GNSS Service (IGS) [13]. However, due to a 15-day latency in the availability of IGS satellite clock and orbit products, early studies on PPP focused on postprocessing applications. As the demand for real-time (RT) PWV sensing and positioning increased [14], [15], research on RT PPP processing addressed related challenges. One of the main studied issues is RT estimation of the GNSS satellite clock error [16], [17], [18], [19], [20], [21], [22], considering that the IGS ultrarapid (IGU) orbit product is precise enough to achieve high-precision atmospheric water vapor estimation and centimeter-level positioning. Estimation methods for the GNSS satellite clock error typically utilize dual-frequency phase and range observations from a global or regional GNSS network.

The IGS provides the real-time service (RTS) for the GNSS satellite orbit and clock corrections with respect to broadcast ephemeris [23], [24], [25]. The RTS, established in 2011, provides satellite orbit and clock corrections to RT PPP users via the internet at high-frequency update intervals [26]. The frequent updates of correction coefficients depend on the connectivity between the PPP user and the server hosting the satellite clock and orbit products. However, connectivity can be disrupted by unforeseen events such as heavy rainstorms. In such cases, it becomes crucial to maintain high-precision RT PPP processing and ensure accurate sensing of atmospheric water vapor. To address this challenge, Li et al. [27], [28] proposed an improved RTS method with a prolonged update interval of satellite clock corrections, 12 times longer than that of IGS RTS. While this approach enhances the RTS performance and is implemented on the RTS server, it still relies on stable connectivity.

In [29], the combined corrections are computed by selecting ionosphere-free combinations from the reference network. However, this approach requires the construction of a new RTS server and does not address communication breaks at the PPP user's end. El-Mowafy et al. [30] propose a method that utilizes the open-access IGS RTS product to predict precise orbit and clock corrections as time series. This method enables RT PPP with 3-D accuracy of less than a decimeter even when communication is disconnected. The prediction algorithm extrapolates subsequent values based on the previous satellite clock and orbit corrections. Therefore, it is necessary to store the previous satellite clock and

Manuscript received 26 May 2023; revised 2 July 2023 and 26 August 2023; accepted 2 September 2023. Date of publication 6 September 2023; date of current version 18 September 2023. This work was supported by the National Natural Science Foundation of China under Grant 41974025 and Grant 42174019, and in part by the Fundamental Research Funds for the Central Universities. *(Corresponding author: XiaoMing Li.)*

HaoJun Li and XiaoMing Li are with the College of Surveying and Geo-Informatics, Tongji University, Shanghai 200092, China (e-mail: lhjch@tongji.edu.cn; lxmch@tongji.edu.cn).

Qi Kang is with the Department of Control Science and Engineering, Tongji University, Shanghai 200092, China (e-mail: qkang@tongji.edu.cn).

Digital Object Identifier 10.1109/JSTARS.2023.3312514

orbit corrections at the RT PPP user, which requires additional memory space. It should be noted that RT GNSS PPP for atmospheric water vapor sensing is not limited to personal computers but is also embedded in various mobile devices like cell phones to cater to different requirements. To reduce computational and storage costs, it is crucial to determine the optimal arc length of the satellite clock correction series used for high-precision extrapolation. Using the shortest and most suitable arc length can significantly optimize computation and storage requirements. Therefore, studying the effect of the arc length of the satellite clock correction series on extrapolation results is important. Nie et al. [31] propose a method that does not require saving received RTS clock corrections but has lower accuracy compared to RTS. Hence, it is important to develop a method that saves memory space while maintaining the accuracy of RT PPP for atmospheric water vapor sensing during discontinuities at the PPP user's end. In this study, a handling method for outages of IGS RTS in RT sensing of atmospheric water vapor in PPP is proposed and discussed. This method presents an optimal strategy for saving the appropriate IGS RTS satellite clock corrections to maintain the accuracy of RT sensing of atmospheric water vapor. Additionally, by utilizing IGU products, it avoids the requirement to store previous satellite orbit corrections and reduces the dependence on connectivity.

II. Methodology and Data

A. RT PPP for Outages of IGS RTS

PPP processing commonly utilizes the ionosphere-free combination of pseudorange and carrier phase observations.

$$\begin{cases} P_r^s = \rho_r^s + c\,(dt_r - dt^s) + c\,(b_r - b^s) \\ + (mf_h \times \mathrm{ZHD} + mf_w \times \mathrm{ZWD}) + \varepsilon_r^s \\ L_r^s = \rho_r^s + c\,(dt_r - dt^s) + \lambda_{IF}\,(N_r^s + B_r - B^s) \\ + (mf_h \times \mathrm{ZHD} + mf_w \times \mathrm{ZWD}) + \epsilon_r^s \end{cases} \tag{1}$$

where P_r^s and L_r^s represent ionospheric-free observations of pseudorange and carrier phase of receiver r and satellite s; ρ_r^s is the geometric distance from the satellite to the receiver; dt_r and dt^s represent receiver clock error and satellite clock error; b_r and b^s are the receiver and satellite hardware delay bias, respectively, in pseudorange observation; B_r and B^s are the receiver and satellite phase delay bias, respectively; N_r^s is the integer ionosphere-free phase ambiguity and λ_{IF} is its wavelength; ZHD and ZWD are the tropospheric zenith hydrostatic delay and wet delay, respectively, and mf_h and mf_w are their corresponding mapping function; and ε_r^s and ϵ_r^s represent pseudorange and phase observation noises, respectively.

In RT PPP, GNSS users receive RT high-precision satellite clock and orbit corrections transmitted by various global RT analysis centers (ACs). These ACs, such as CNES, CAS, DLR/GSOC, GFZ, GMV, and WUHAN, provide correction products for GPS, BDS3, GLONASS, and Galileo systems [23], [32]. The update interval for IGS RTS is typically 5 s. To achieve high-precision PPP and atmospheric water vapor sensing, users rely on consistent connectivity to receive accurate correction products. However, during communication interruptions caused by extreme events like earthquakes, users may not receive RT data streams from IGS. While the orbit accuracy of IGU products can reach centimeter-level precision [19], [20], the satellite clock corrections have lower precision. To address this issue, a method has been established that employs an extrapolation algorithm. Once communication is interrupted, this method utilizes the saved historical clock correction values of the user and constructs a function based on the periodic characteristics of satellite clock [33], [34], [35]. The extrapolation algorithm takes advantage of these characteristics to predict satellite clock corrections during the interruption. It is written as follows:

$$dt^s\ (t) = a_0 + \sum_{k=1}^{n} \left(a_k \times t^k\right) + \sum_{i=1}^{n_1} \mathrm{A}_i \times \sin\left(\frac{2\pi}{T_i} \times t + \Phi_i\right) \tag{2}$$

where t is the time; $dt^s(t)$ is the satellite clock correction at t; a_0 and a_k $(k = 1, n)$ are the polynomial coefficients, n is the order of the polynomial; n_1 is the number of main periodic terms; i is the harmonic order; and T_i, A_i, and Φ_i are the period, amplitude, and initial phase, respectively. In contrast to the current application method, we employ this function to establish a high-precision RTS for satellite clock correction. Additionally, we analyze the suitable arc length of the satellite clock correction series to optimize the memory space usage. When communication is interrupted, RT PPP is performed using the IGU satellite orbit and the proposed RTS of satellite clock correction. The tropospheric hydrostatic delay is computed using the Saastamoinen model [36], while the wet delay component is estimated as white noise. The estimated parameters for RT PPP can be expressed as

$$X = \begin{bmatrix} d_x & d_y & d_z & dt_r & \mathrm{ZWD} & \tilde{N} \end{bmatrix}^T \tag{3}$$

where d_x, d_y, d_z represent coordinate error; and $\tilde{N} = N_r^s + B_r - B^s$ refers to float ambiguity, which includes phase hardware delay and misses integer characteristics.

B. RT Atmospheric Water Vapor Retrieval

When dealing with outages of IGS RTS, the RT PPP processing can be carried out as usual and the RT PWV can be obtained using the estimated ZWD of RT PPP. It is expressed as [37]

$$\mathrm{PWV} = \frac{10^6}{\left(k_2' + \frac{k_3}{T_m}\right) \cdot R_v \cdot \rho_{lw}} \cdot \mathrm{ZWD} \tag{4}$$

where $k_2' = (17 \pm 10)\ \mathrm{K} \cdot \mathrm{hP}a^{-1}$ and $k_3 = (3.776 \pm 0.004)10^5 \mathrm{K}^2 \cdot \mathrm{hP}a^{-1}$ are atmospheric refractivity constants, respectively, R_v is water vapor specific gas constant$(461.495\ \mathrm{J} \cdot (\mathrm{kg} \cdot \mathrm{K})^{-1})$, and ρ_{lw} represents liquid water density. T_m represents weighted-mean-temperature, which can be derived based from ERA5 layer or measured meteorological data [38], [39], [40]. Fig. 1 shows the flow chart of RT PWV retrieval in the case of connectivity interruption.

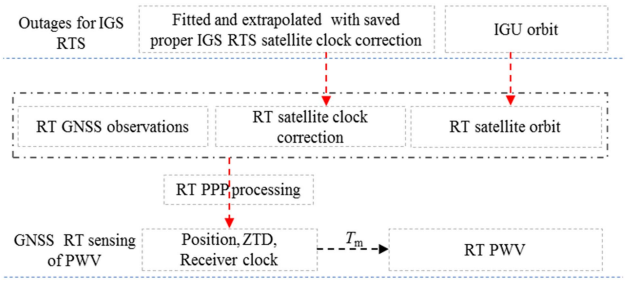

Fig. 1. Flow chart for RT sensing of PWV.

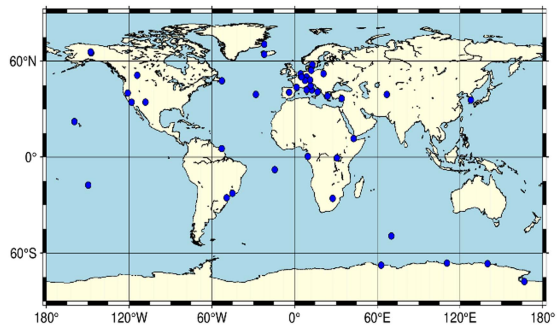

Fig. 2. Distribution of 45 IGS stations.

C. GNSS Data

Four days (August 31, 2022 to September 3, 2022) RT satellite clock correction archived products,[1] broadcast ephemeris, and IGU products are used to simulate the RTS strategy during communication interruption. A total of 45 IGS stations are selected to verify the accuracy of the established method, which includes the RTS of the satellite clock correction, used saved historical clock correction values and extrapolation function, and its performance in RT sensing of atmospheric water vapor for outages of IGS RTS. The distribution of selected stations that provide observations toward GPS, BDS-3, and Galileo is shown in Fig. 2.

III. Results and Analysis

A. RT Satellite Clock Correction

In the case of communication interruption, three strategies are discussed to determine the optimal extrapolation method, considering the appropriate function and arc length of the historical IGS RTS satellite clock correction data saved at the user's end. These strategies involve fitting and extrapolating the satellite clock values with a combined quadratic polynomial and eighth-order harmonic-based function [27]. The strategy of 1# uses recovered satellite clock correction with IGS RTS and broadcast ephemeris, 2# uses IGS RTS values, and 3# uses the difference between the recovered satellite clock correction and that of IGU. The user then performs RT PPP processing using the extrapolated satellite clock correction and the IGU orbit. The performance of the RT PPP is compared among the three strategies to validate the established RTS for satellite clock correction.

[1][Online]. Available: http://www.ppp-wizard.net/products/REAL_TIME/

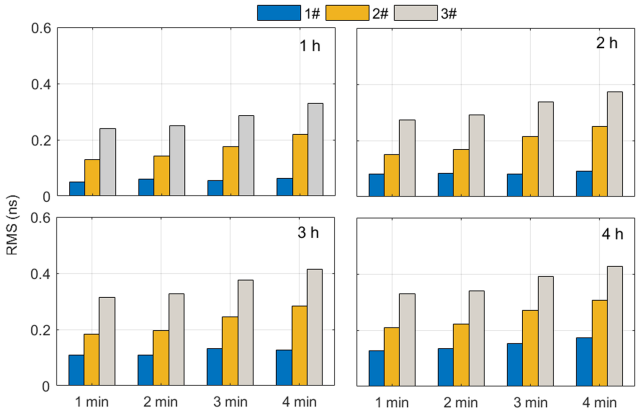

Fig. 3. Averaged RMSE of all extrapolated GPS clock correction of different arcs when connectivity is interrupted.

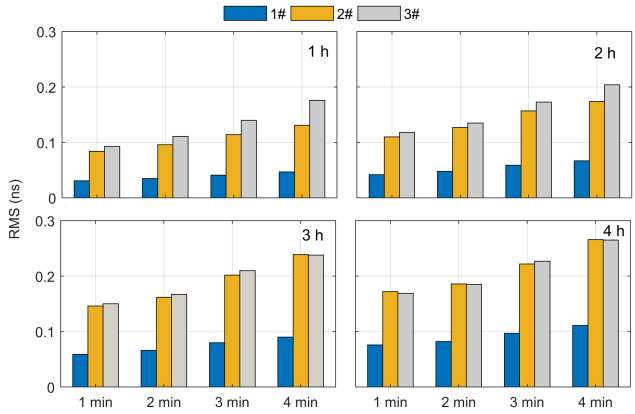

Fig. 4. Averaged RMSE of all extrapolated Galileo clock correction of different arcs when connectivity is interrupted.

To address the issue of connectivity interruptions preventing the RT PPP user from receiving the RTS stream of satellite clock correction, a short-term clock correction extrapolation model is developed to maintain the accuracy of the RT PPP. Different degrees of communication interruption are simulated by using satellite clock correction extrapolation intervals of 1, 2, 5, and 10 min, these mean the interruptions per day is executed every 1, 2, 5, and 10 min, respectively. Figs. 3–5 display the averaged rms error (RMSE) results for GPS, Galileo, and BDS-3 satellite clock corrections using 1, 2, 3, and 4 h of historical values for fitting and extrapolation, with connectivity interruptions of 1, 2, 5, and 10 min. The results indicate that Strategy 1#, which utilizes the recovered satellite clock correction from IGS RTS and broadcast ephemeris, outperforms Strategies 2# and 3# for different extrapolation times and GNSS systems.

It was seen that the averaged RMSE of satellite clock correction for the 1-h historical data is the best and less than 0.2 ns, where the rms results were calculated using G01, E02, and C19 as reference satellite. For GPS, the averaged RMSEs of all satellite clock corrections for three days are 0.112, 0.126,

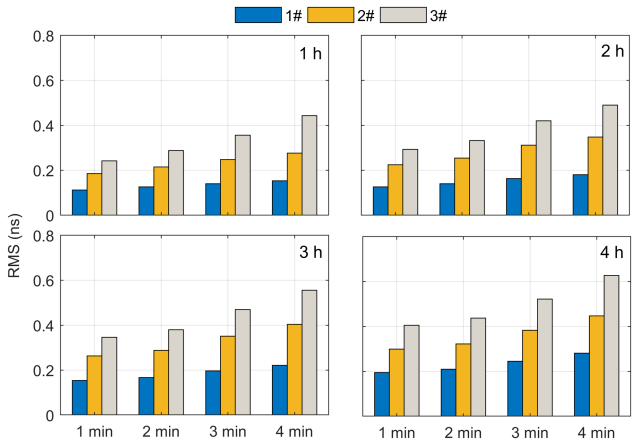

Fig. 5. Averaged RMSE of all extrapolated BDS-3 clock correction of different arcs when connectivity is interrupted.

0.140, and 0.153 ns for four interruptions, respectively. For Galileo, these results are 0.031, 0.035, 0.041, and 0.047 ns, respectively, and those of BDS-3 are 0.051, 0.054, 0.061, and 0.064 ns, respectively. These findings demonstrate that saving the 1-h IGS RTS satellite clock correction for extrapolation is effective in maintaining the accuracy of the RT satellite clock correction and handling outages of IGS RTS. Building upon the performance of Strategy 1#, which employs the saved 1-h IGS RTS satellite clock correction, further analysis is conducted on the RT PPP and the corresponding estimation of atmospheric water vapor.

The performance of the RT satellite clock correction generated by strategy 1# is assessed in kinematic and static PPP processing under different degrees of connectivity interruptions. The assessment is conducted using observation data from selected IGS stations with a sampling interval of 30 s. The Saastamoinen model is employed to calculate the hydrostatic delay and wet delay, and the residual part of the wet delay is estimated along with position, phase ambiguity, and receiver clock error. The meteorological parameters are derived from the GPT2_5w model [41], and the mapping function used is Vienna Mapping Functions 3 (VMF3) [42]. Tables I–IV provide the averaged RMSEs and static averaged convergence times for GPS, Galileo, and BDS-3 PPP using different extrapolated results of the satellite clock correction and archived National Centre for Space Studies (CNES) RT satellite clock products. The static convergence condition is defined as having a continuous position error of less than 10 cm in the North and East directions, and less than 15 cm in the Up direction. The results demonstrate that the PPP positioning error in all directions increases as the IGS RTS interruption time increases. This indicates that longer connectivity interruptions have a greater impact on the accuracy of PPP positioning. The static PPP achieves centimeter-level accuracy, while the kinematic PPP reaches decimeter-level accuracy. The PPP positioning error using strategy 1# is slightly worse than the RTS satellite clock products when outages of IGS RTS lasts for 1 to 10 min, which averaged 3-D RMSE of GPS, BDS-3, and Galileo static

TABLE I
AVERAGED RMSE OF GPS KINEMATIC AND STATIC PPP WITH DIFFERENT SCHEMES (UNIT: M, WHERE 2-D DENOTES TWO DIMENSIONS AND 3-D DENOTES THREE DIMENSIONS, AND "CNES" REPRESENT THE RESULT CALCULATED BY PPP PROCESSING USING CNES RT ARCHIVED PRODUCT)

Mode	Scheme	East	North	Up	2-D	3-D
Static	CNES	0.032	0.017	0.041	0.038	0.057
	1 min	0.030	0.018	0.044	0.036	0.060
	2 min	0.032	0.019	0.045	0.038	0.062
	5 min	0.036	0.019	0.051	0.042	0.069
	10 min	0.038	0.021	0.051	0.044	0.070
Kinematic	CNES	0.095	0.062	0.181	0.116	0.217
	1 min	0.098	0.084	0.227	0.131	0.264
	2 min	0.120	0.100	0.266	0.158	0.311
	5 min	0.149	0.123	0.315	0.196	0.374
	10 min	0.163	0.138	0.353	0.217	0.418

TABLE II
AVERAGED RMSE OF GALILEO KINEMATIC AND STATIC PPP WITH DIFFERENT SCHEMES (UNIT: M, WHERE 2-D DENOTES TWO DIMENSIONS AND 3-D DENOTES THREE DIMENSIONS)

Mode	Scheme	East	North	Up	2-D	3-D
Static	CNES	0.059	0.027	0.061	0.067	0.093
	1 min	0.061	0.028	0.063	0.069	0.096
	2 min	0.062	0.028	0.064	0.070	0.098
	5 min	0.064	0.029	0.066	0.072	0.100
	10 min	0.065	0.030	0.069	0.075	0.105
Kinematic	CNES	0.177	0.209	0.435	0.289	0.529
	1 min	0.180	0.217	0.454	0.296	0.549
	2 min	0.181	0.216	0.457	0.296	0.552
	5 min	0.183	0.222	0.467	0.302	0.562
	10 min	0.187	0.227	0.481	0.307	0.577

PPP have only decreased by 5%, 3.1%, and 1.6%, respectively, when interruption lasts for 1 min, 17.8%, 3.6%, and 2.1% for simulated kinematic PPP, respectively. Table IV confirms that longer connectivity interruptions result in longer convergence times for PPP. Figs. 6–8 provide static and kinematic GPS, Galileo, and BDS-3 PPP results for station FFMJ. These figures

TABLE III
AVERAGED RMSE OF BDS-3 KINEMATIC AND STATIC PPP WITH DIFFERENT SCHEMES (UNIT: M, WHERE 2-D DENOTES TWO DIMENSIONS AND 3-D DENOTES THREE DIMENSIONS)

MODE	Scheme	East	North	Up	2-D	3-D
Static	CNES	0.091	0.035	0.068	0.100	0.125
	1 min	0.091	0.035	0.072	0.100	0.127
	2 min	0.092	0.035	0.073	0.101	0.128
	5 min	0.091	0.036	0.073	0.100	0.129
	10 min	0.094	0.036	0.072	0.104	0.131
Kinematic	CNES	0.626	0.543	1.441	0.862	1.719
	1 min	0.635	0.551	1.477	0.876	1.756
	2 min	0.610	0.511	1.281	0.829	1.561
	5 min	0.613	0.533	1.374	0.850	1.656
	10 min	0.613	0.515	1.291	0.834	1.572

TABLE IV
AVERAGED CONVERGENCE TIMES WITH DIFFERENT SCHEMES UNDER CONNECTIVITY INTERRUPTIONS (UNIT: MIN)

Scheme	GPS	Galileo	BDS-3
CNES	31.6	52.7	63.2
1 min	63.4	58.4	80.1
2 min	66.5	60.7	81.8
5 min	75.8	72.2	103.5
10 min	82.2	73.3	115.8

demonstrate that when communication is interrupted for 1, 2, 5, and 10 min, the extrapolated GPS, Galileo, and BDS-3 satellite clock correction can achieve static positioning accuracy at the centimeter or even millimeter level, and kinematic positioning accuracy at the decimeter to centimeter level. Compared with the archived satellite clock products, the proposed strategy has good consistency in static and kinematic PPP positioning sequence except for GPS. Although communication outages lead to a greater impact on convergence time for GPS kinematic PPP, centimeter, or even millimeter level positioning can be achieved for GPS static PPP. The proposed strategy for short-term IGS RTS outages performs better on maintaining the positioning accuracy of BDS-3 and Galileo. These results indicate that the

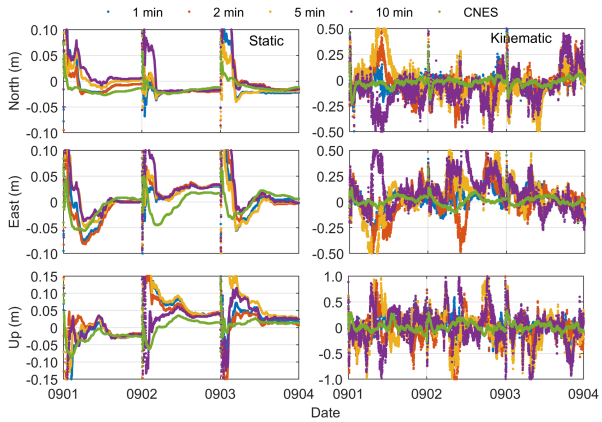

Fig. 6. Three-day static and kinematic GPS PPP results (m) for station FFMJ under connectivity interruptions of different degrees.

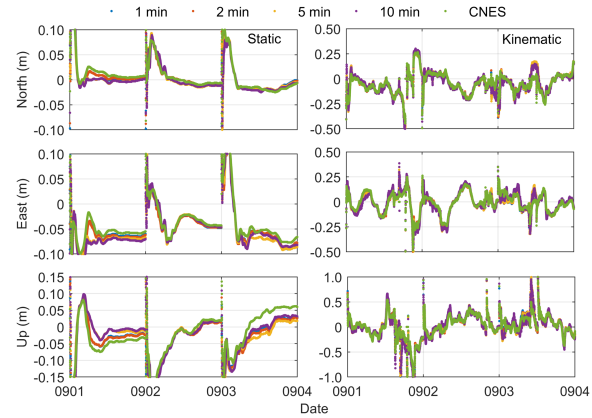

Fig. 7. Three-day static and kinematic Galileo PPP results (m) for station FFMJ under connectivity interruptions of different degrees.

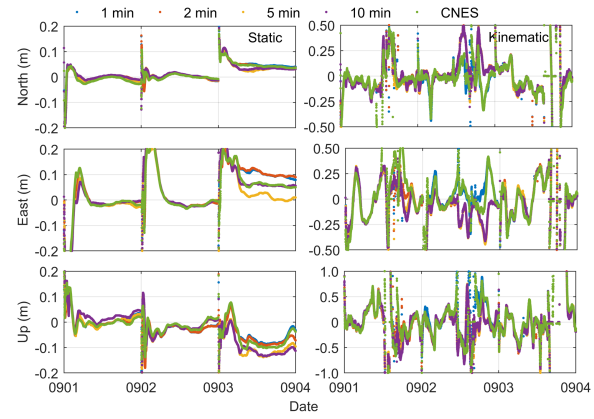

Fig. 8. Three-day static and kinematic BDS-3 PPP results (m) for station FFMJ under connectivity interruptions of different degrees.

handling method, constructed based on the extrapolation algorithm of the combined quadratic polynomial and eighth-order harmonic-based function, can maintain good positioning accuracy in cases of sudden connectivity interruption. Indeed, this approach allows for the continuation of precise positioning and reduces the impact of communication outages on the accuracy of RT positioning solutions.

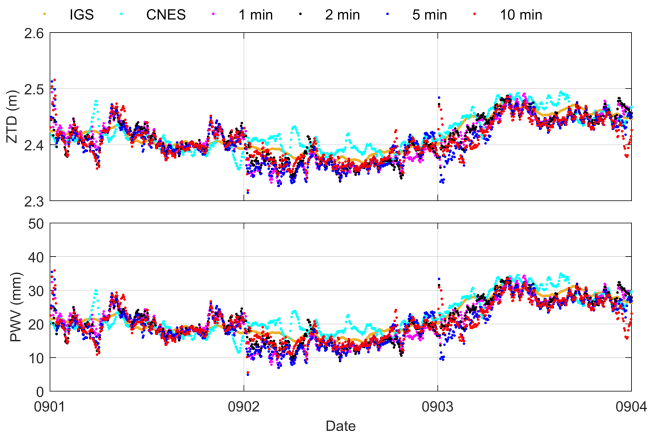

Fig. 9. Three-day GPS ZTD and PWV results for station FFMJ under connectivity interruptions of different degrees ("IGS" represent final product provided by IGS, and "CNES" represent the result calculated by PPP processing using CNES RT archived product).

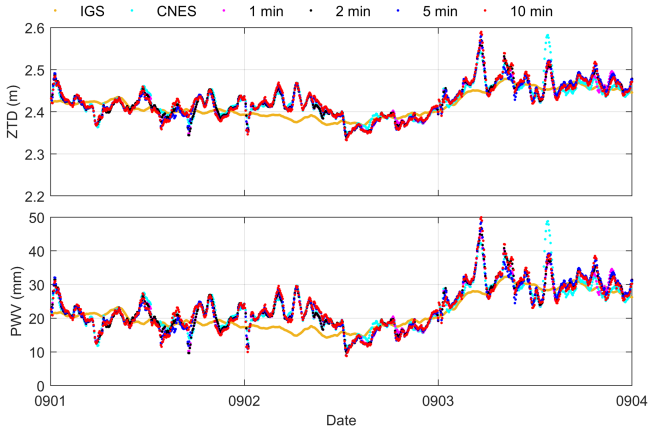

Fig. 10. Three-day Galileo ZTD and PWV results for station FFMJ under connectivity interruptions of different degrees ("IGS" represent final product provided by IGS, and "CNES" represent the result calculated by PPP processing using CNES RT archived product).

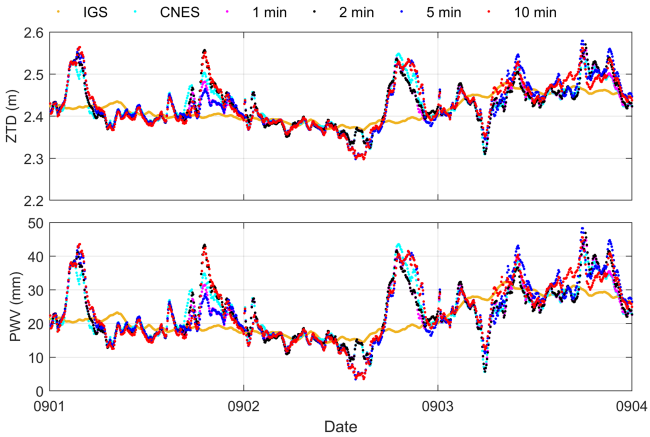

Fig. 11. Three-day BDS-3 ZTD and PWV results for station FFMJ under connectivity interruptions of different degrees ("IGS" represent final ZTD product provided by IGS, and "CNES" represent the result calculated by PPP processing using CNES RT archived product).

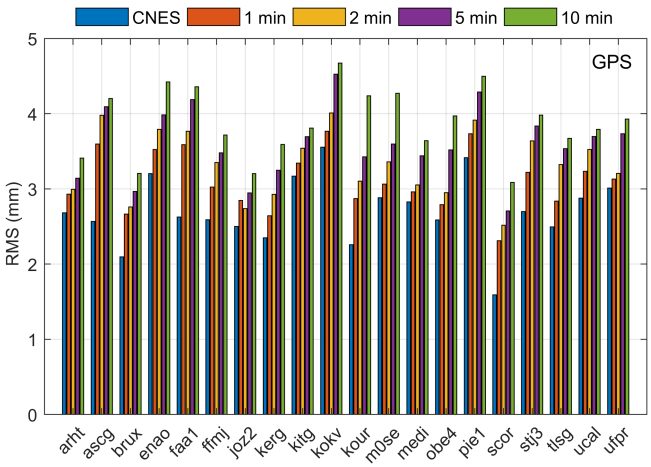

Fig. 12. RMS of different schemes for GPS PWV.

B. Atmospheric Water Vapor

The performance of the handling method in sensing of atmospheric water vapor during communication interruption is evaluated by estimating the RT zenith tropospheric delay (ZTD) using RT PPP processing. The corresponding PWV is then obtained based on the procedure outlined in Fig. 1. These estimated results for different degrees of connectivity interruption are compared with the IGS postprocessing products, which are obtained from the archived product of CNES [43].

Figs. 9–11 provide the ZTD and PWV results of GPS, Galileo, and BDS-3 for the FFMJ station over three consecutive days. These figures illustrate that the differences between the estimated results under different degrees of connectivity interruption are minimal. Comparing these results with the IGS products, it is observed that GPS has the highest accuracy, followed by Galileo and BDS-3. Furthermore, the PWV results for different degrees of connectivity interruption are found to be comparable to the CNES products. These performances indicate that the developed method for handling outages of IGS RTS can maintain a stable accuracy in PWV estimation, even during several minutes of communication interruption. To further analyze the accuracy of ZTD estimation, the rms, STD, and MEAN values of ZTD are computed for GPS, Galileo, and BDS-3 observations for all 45 stations. The results are compared with the different degrees of connectivity interruption, CNES products, and IGS products, and presented in Table V. The table demonstrates that the accuracy of ZTD estimation for each satellite system decreases as the connectivity interruption time increases. Table VI presents the PWV estimation results, indicating that the accuracy of PWV estimation for GPS, Galileo, and BDS-3 under different degrees of connectivity interruption remains at the millimeter level. Even when the connectivity interruption lasts for 10 min, the water vapor retrieval performance is comparable to that of the CNES RT clock products.

Figs. 12–14 display the rms values of PWV differences for GPS, Galileo, and BDS-3 under different degrees of connectivity interruption for the selected 20 IGS stations. The figures

TABLE V
COMPARISON BETWEEN DIFFERENT SCHEMES AND IGS ZTD PRODUCTS (UNIT: CM)

System	Scheme	RMS	STD	MEAN
GPS	CNES	1.87	1.65	-0.15
	1 min	1.99	1.77	-0.17
	2 min	2.04	1.82	-0.18
	5 min	2.13	1.89	-0.27
	10 min	2.20	1.99	-0.27
Galileo	CNES	2.72	2.42	0.10
	1 min	2.94	2.66	0.10
	2 min	2.97	2.69	0.12
	5 min	3.03	2.74	0.09
	10 min	3.07	2.78	0.11
BDS-3	CNES	3.98	3.68	0.53
	1 min	4.06	3.77	0.50
	2 min	4.13	3.82	0.55
	5 min	4.23	3.93	0.46
	10 min	4.21	3.90	0.39

TABLE VI
COMPARISON BETWEEN DIFFERENT SCHEMES PWV AND IGS ZTD PRODUCTS PWV (UNIT: MM)

System	Scheme	RMS	STD	MEAN
GPS	CNES	2.91	2.51	0.26
	1 min	3.12	2.75	0.26
	2 min	3.18	2.82	0.31
	5 min	3.26	2.93	0.39
	10 min	3.42	3.12	0.36
Galileo	CNES	4.09	3.79	-0.09
	1 min	4.41	4.12	-0.17
	2 min	4.45	4.15	-0.20
	5 min	4.52	4.22	-0.16
	10 min	4.57	4.26	-0.20
BDS-3	CNES	6.29	5.80	-0.89
	1 min	6.43	5.96	-0.83
	2 min	6.54	6.03	-0.91
	5 min	6.70	6.21	-0.76
	10 min	6.66	6.16	-0.65

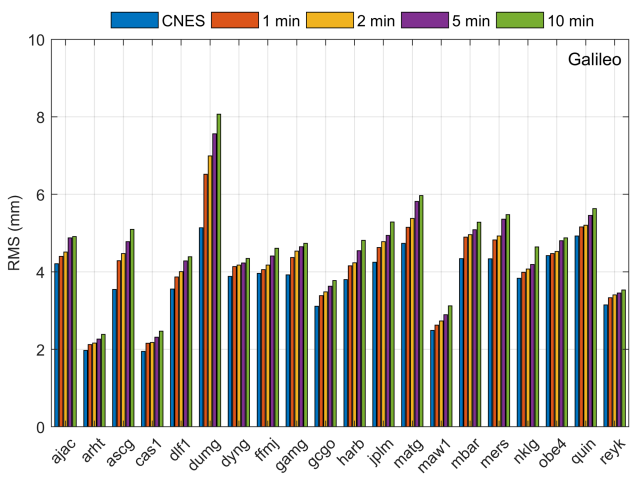

Fig. 13. RMS of different schemes for Galileo PWV.

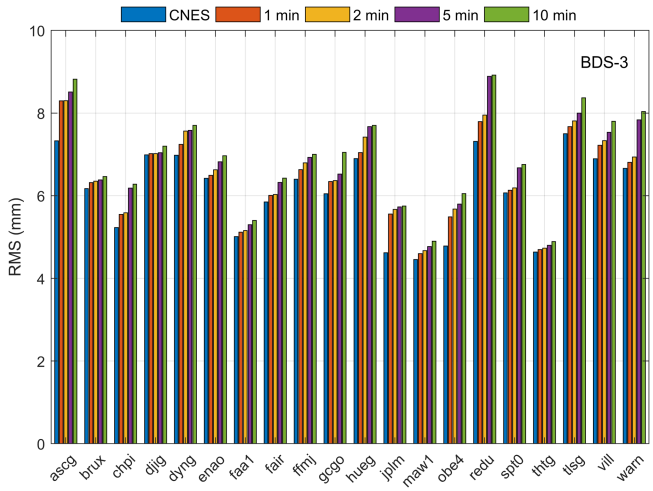

Fig. 14. RMS of different schemes for BDS-3 PWV.

indicate that the rms values of PWV differences are generally better than 5 mm for GPS, with most stations achieving this level of accuracy. For Galileo, the majority of stations also achieve a PWV rms value better than 5 mm. In the case of BDS-3, most stations can achieve a PWV rms value better than 8 mm. These PWV retrieving results further confirm the feasibility of the constructed RTS of the satellite clock correction when connectivity is interrupted for several minutes. The performance observed in these results meets the accuracy requirements of medium or long-term numerical weather forecasts, validating the potential usefulness of the method in practical applications [44].

IV. Conclusion

In this study, a method for GNSS sensing of atmospheric water vapor is proposed to address the issue of outages in IGS RTS caused by natural hazards. The method utilizes the IGU satellite orbit product and a constructed RTS of satellite clock correction. The performance of the constructed RTS of satellite clock correction is evaluated. The results demonstrate that the satellite clock correction for GPS, Galileo, and BDS-3 can achieve accuracies of 0.112, 0.031, and 0.051 ns, respectively, even when connectivity is interrupted for several minutes. Moreover, the static PPP achieves millimeter-level positioning accuracy, while the kinematic PPP achieves decimeter to centimeter-level positioning accuracy. These PPP performances ensure the estimation accuracy of PWV, allowing for reliable GNSS sensing of atmospheric water vapor.

The comparison of the averaged rms values of ZTD and PWV estimated by GPS, Galileo, and BDS-3 with the IGS products shows promising results. The averaged rms values of ZTD estimated by GPS, Galileo, and BDS-3 at different connectivity interruption degrees are reported to be 1.99, 2.94, and 4.06 cm, respectively. Similarly, the averaged rms values of PWV for GPS, Galileo, and BDS-3 are 3.12, 4.41, and 6.43 mm, respectively. These indicate that established method can contribute to handling outages of IGS RTS in RT GNSS atmospheric PWV estimation, and meet the accuracy requirements of general numerical weather prediction applications.

References

[1] S. Malys and P. A. Jensen, "Geodetic point positioning with GPS carrier beat phase data from the CASA UNO Experiment," *Geophys. Res. Lett.*, vol. 17, no. 5, pp. 651–654, Apr. 1990.

[2] J. F. Zumberge, M. B. Heflin, D. C. Jefferson, M. M. Watkins, and F. H. Webb, "Precise point positioning for the efficient and robust analysis of GPS data from large networks," *J. Geophys. Res.*, vol. 102, no. B3, pp. 5005–5017, Mar. 1997.

[3] L. Chen, F. Zheng, X. Gong, and X. Jiang, "GNSS high-precision augmentation for autonomous vehicles: Requirements, solution, and technical challenges," *Remote Sens.*, vol. 15, no. 6, Mar. 2023, Art. no. 1623.

[4] X. Li et al., "Multi-GNSS meteorology: Real-time retrieving of atmospheric water vapor from BeiDou, galileo, GLONASS, and GPS observations," *IEEE Trans. Geosci. Remote Sens.*, vol. 53, no. 12, pp. 6385–6393, Dec. 2015.

[5] C. Lu et al., "Real-time retrieval of precipitable water vapor from galileo observations by using the MGEX network," *IEEE Trans. Geosci. Remote Sens.*, vol. 58, no. 7, pp. 4743–4753, Jul. 2020.

[6] Z. Wu et al., "Sensing real-time water vapor over oceans with low-cost GNSS receivers," *IEEE Trans. Geosci. Remote Sens.*, vol. 60, 2022, Art. no. 5804208.

[7] J. Geng, Y. Bock, D. Melgar, B. W. Crowell, and J. S. Haase, "A new seismogeodetic approach applied to GPS and accelerometer observations of the 2012 Brawley seismic swarm: Implications for earthquake early warning," *Geochem., Geophys., Geosyst.*, vol. 14, no. 7, pp. 2124–2142, 2013.

[8] R. Fang, C. Shi, W. Song, G. Wang, and J. Liu, "Determination of earthquake magnitude using GPS displacement waveforms from real-time precise point positioning," *Geophys. J. Int.*, vol. 196, no. 1, pp. 461–472, Jan. 2014.

[9] X. Tang, G. W. Roberts, X. Li, and C. M. Hancock, "Real-time kinematic PPP GPS for structure monitoring applied on the severn suspension bridge, U.K.," *Adv. Space Res.*, vol. 60, no. 5, pp. 925–937, Sep. 2017.

[10] T. Hadas, T. Hobiger, and P. Hordyniec, "Considering different recent advancements in GNSS on real-time zenith troposphere estimates," *GPS Solutions*, vol. 24, no. 4, Oct. 2020, Art. no. 99.

[11] J. Askne and H. Nordius, "Estimation of tropospheric delay for microwaves from surface weather data," *Radio Sci.*, vol. 22, no. 3, pp. 379–386, May 1987.

[12] M. Bevis, S. Businger, T. A. Herring, C. Rocken, R. A. Anthes, and R. H. Ware, "GPS meteorology: Remote sensing of atmospheric water vapor using the global positioning system," *J. Geophys. Res.*, vol. 97, no. D14, 1992, Art. no. 15787.

[13] J. M. Dow, R. E. Neilan, and C. Rizos, "The international GNSS service in a changing landscape of global navigation satellite systems," *J. Geodesy*, vol. 83, no. 3–4, pp. 191–198, Mar. 2009.

[14] Q. Zhao, Y. Liu, X. Ma, W. Yao, Y. Yao, and X. Li, "An improved rainfall forecasting model based on GNSS observations," *IEEE Trans. Geosci. Remote Sens.*, vol. 58, no. 7, pp. 4891–4900, Jul. 2020.

[15] Y. Yuan et al., "Real-time retrieval of precipitable water vapor from GPS precise point positioning," *J. Geophys. Res., D. Atmospheres*, vol. 119, no. 16, pp. 10043–10057, 2014.

[16] Q. Zhang, P. Moore, J. Hanley, and S. Martin, "Auto-BAHN: Software for near real-time GPS orbit and clock computations," *Adv. Space Res.*, vol. 39, no. 10, pp. 1531–1538, Jan. 2007.

[17] A. Hauschild and O. Montenbruck, "Kalman-filter-based GPS clock estimation for near real-time positioning," *GPS Solutions*, vol. 13, no. 3, pp. 173–182, Jul. 2009.

[18] H. Bock, R. Dach, A. Jäggi, and G. Beutler, "High-rate GPS clock corrections from CODE: Support of 1 Hz applications," *J. Geodesy*, vol. 83, no. 11, pp. 1083–1094, Nov. 2009.

[19] H. Li, J. Chen, J. Wang, C. Hu, and Z. Liu, "Network based real-time precise point positioning," *Adv. Space Res.*, vol. 46, no. 9, pp. 1218–1224, Nov. 2010.

[20] H. Li, J. Wang, J. Chen, C. Hu, and H. Wang, "The realization and analysis of GNSS Network based Real-time Precise Point Positioning," *Chin. J. Geophys*, vol. 53, no. 6, pp. 1302–1307, Jun. 2010.

[21] X. Zhang, X. Li, and F. Guo, "Satellite clock estimation at 1 Hz for realtime kinematic PPP applications," *GPS Solutions*, vol. 15, no. 4, pp. 315–324, Oct. 2011.

[22] M. Ge, J. Chen, J. Douša, G. Gendt, and J. Wickert, "A computationally efficient approach for estimating high-rate satellite clock corrections in realtime," *GPS Solutions*, vol. 16, no. 1, pp. 9–17, Jan. 2012.

[23] M. Elsobeiey and S. Al-Harbi, "Performance of real-time precise point positioning using IGS real-time service," *GPS Solutions*, vol. 20, no. 3, pp. 565–571, Jul. 2016.

[24] Y. Du, J. Wang, C. Rizos, and A. El-Mowafy, "Vulnerabilities and integrity of precise point positioning for intelligent transport systems: Overview and analysis," *Satell. Navigation*, vol. 2, no. 1, Dec. 2021, Art. no. 3.

[25] Y. Wang and J. Shen, "Real-time integrity monitoring for a wide area precise positioning system," *Satell. Navigation*, vol. 1, no. 1, Dec. 2020, Art. no. 24.

[26] M. Caissy, L. Agrotis, G. Weber, M. Hernandez-Pajares, and U. Hugentobler, "The international GNSS real-time service," *GPS World*, vol. 23, no. 6, pp. 52–58, 2012.

[27] H. Li, X. Li, and X. Gong, "Improved method for the GPS high-precision real-time satellite clock error service," *GPS Solutions*, vol. 26, no. 4, Oct. 2022, Art. no. 136.

[28] H. Li, H. Ding, B. Feng, and Q. Kang, "Improved method for BDS-3 satellite clock parameterization in the broadcast ephemeris, real-time service (RTS) and IGS final products," *Measurement*, vol. 204, Nov. 2022, Art. no. 112059.

[29] Q. Zhao, W. Gao, C. Gao, S. Pan, X. Yang, and J. Wang, "Comprehensive outage compensation of real-time orbit and clock corrections with broadcast ephemeris for ambiguity-fixed precise point positioning," *Adv. Space Res.*, vol. 67, no. 3, pp. 1124–1142, Feb. 2021.
[30] A. El-Mowafy, M. Deo, and N. Kubo, "Maintaining real-time precise point positioning during outages of orbit and clock corrections," *GPS Solutions*, vol. 21, no. 3, pp. 937–947, Jul. 2017.
[31] Z. Nie, Y. Gao, Z. Wang, S. Ji, and H. Yang, "An approach to GPS clock prediction for real-time PPP during outages of RTS stream," *GPS Solutions*, vol. 22, no. 1, Jan. 2018, Art. no. 14.
[32] B. Li, H. Ge, Y. Bu, Y. Zheng, and L. Yuan, "Comprehensive assessment of real-time precise products from IGS analysis centers," *Satell. Navigation*, vol. 3, no. 1, Dec. 2022, Art. no. 12.
[33] K. L. Senior, J. R. Ray, and R. L. Beard, "Characterization of periodic variations in the GPS satellite clocks," *GPS Solutions*, vol. 12, no. 3, pp. 211–225, Jul. 2008.
[34] H. Li, X. Liao, B. Li, and L. Yang, "Modeling of the GPS satellite clock error and its performance evaluation in precise point positioning," *Adv. Space Res.*, vol. 62, no. 4, pp. 845–854, Aug. 2018.
[35] X. Yan, W. Li, Y. Yang, and X. Pan, "BDS satellite clock offset prediction based on a semiparametric adjustment model considering model errors," *Satell. Navigation*, vol. 1, no. 1, Dec. 2020, Art. no. 11.
[36] J. Saastamoinen, "Contributions to the theory of atmospheric refraction," *Bull. Geodesique*, vol. 105, no. 1, pp. 279–298, Sep. 1972.
[37] W. Zhang et al., "On the suitability of ERA5 in hourly GPS precipitable water vapor retrieval over China," *J. Geodesy*, vol. 93, no. 10, pp. 1897–1909, Oct. 2019.
[38] P. Sun, S. Wu, K. Zhang, M. Wan, and R. Wang, "A new global grid-based weighted mean temperature model considering vertical nonlinear variation," *Atmos. Meas. Tech.*, vol. 14, no. 3, pp. 2529–2542, Mar. 2021.
[39] P. Sun, K. Zhang, S. Wu, R. Wang, D. Zhu, and L. Li, "An investigation of a voxel-based atmospheric pressure and temperature model," *GPS Solutions*, vol. 27, no. 1, Jan. 2023, Art. no. 56.
[40] P. Jiang, S. Ye, Y. Lu, Y. Liu, D. Chen, and Y. Wu, "Development of time-varying global gridded Ts-Tm model for precise GPS–PWV retrieval," *Atmos. Meas. Tech.*, vol. 12, no. 2, pp. 1233–1249, Feb. 2019.
[41] J. Böhm, G. Möller, M. Schindelegger, G. Pain, and R. Weber, "Development of an improved empirical model for slant delays in the troposphere (GPT2w)," *GPS Solutions*, vol. 19, no. 3, pp. 433–441, Jul. 2015.
[42] D. Landskron and J. Böhm, "VMF3/GPT3: Refined discrete and empirical troposphere mapping functions," *J. Geodesy*, vol. 92, no. 4, pp. 349–360, Apr. 2018.
[43] L. Zhang, H. Yang, Y. Gao, Y. Yao, and C. Xu, "Evaluation and analysis of real-time precise orbits and clocks products from different IGS analysis centers," *Adv. Space Res.*, vol. 61, no. 12, pp. 2942–2954, Jun. 2018.
[44] D. Offiler, J. Jones, G. Bennit, and H. Vedel, "EIG eumetnet GNSS water vapour programme (E-GVAP-II)," EIG EUMETNET, Brussels, Belgium, Tech. Rep. 1, Dec. 2010. [Online]. Available: http://egvap.dmi.dk/support/formats/egvap_prd_v10.pdf

HaoJun Li received the Ph.D. degree in geodesy from Tongji University, Shanghai, China, in 2010.

He is currently a Professor in geodesy and surveying engineering with Tongji University. His research interests include precise point positioning, satellite clocks, and multi global satellite navigation system and multifrequency biases.

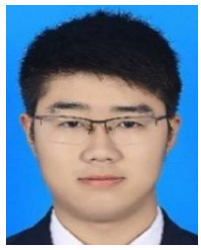

XiaoMing Li received the master's degree in surveying and mapping science and technology from Jiangsu Normal University, Xuzhou, China, in 2019. He is currently working toward the Ph.D. degree in surveying and mapping science and technology with the College of Surveying and Geo-Informatics, Tongji University, Shanghai, China.

His current research interests include global satellite navigation system precise point positioning and satellite clock determination.

Qi Kang (Senior Member, IEEE) received the B.S. degree in automatic control, the M.S. degree in control theory and control engineering, and the Ph.D. degree in control theory and control engineering from Tongji University, Shanghai, China, in 2002, 2005, and 2009, respectively.

From 2007 to 2008, he was a Research Associate with the University of Illinois, Chicago, IL, USA. From 2014 to 2015, he was a Visiting Scholar with the New Jersey Institute of Technology, Newark, NJ, USA. He is currently a Professor with the Department of Control Science and Engineering, Tongji University. His research interests include swarm intelligence, evolutionary computation, machine learning, intelligent control, and optimization in transportation, energy, and water systems